Optics and Lasers in Engineering 152 (2022) 106944

Contents lists available at ScienceDirect

Optics and Lasers in Engineering

journal homepage: www.elsevier.com/locate/optlaseng

Evaluation of wavefront aberrations induced by overlay errors in stitching computer-generated holograms

YingYing Bai[a,b], ZhiYu Zhang[a,*], TianBao Chen[a,b], RuoQiu Wang[a], HongDa Wei[a], XueFeng Zeng[a], XueJun Zhang[a,*]

[a] Key Laboratory of Optical System Advanced Manufacturing Technology, Changchun Institute of Optics, Fine Mechanics and Physics, Chinese Academy of Sciences, Changchun 130033, China
[b] University of Chinese Academy of Sciences, Beijing 100049, China

ARTICLE INFO

Keywords:
Computer-generated hologram
Optical testing
Error analysis

ABSTRACT

The emergence of large-aperture telescopes has fueled the need for testing and assisted alignment of large-scale optical systems. Computer-generated holograms (CGHs) have proven to be a useful method for aspheric optical testing and assisted alignment, and large-sized CGHs are required for large-scale aspherical systems. However, the maximum size of CGH is generally in the range of 6 to 9 inches owing to its current lithography capability. Stitching technology is a promising method for realizing larger-sized CGHs. As a proof of concept, a CGH with an aperture of 80 mm is fabricated using multistep lithography to investigate the overlay errors in stitching. Theoretical derivations reveal that additional tip/tilt aberrations are introduced owing to the overlay errors, which commonly couple with aberrations from adjustment errors. Therefore, to budget the effects of overlay errors, an evaluation method is proposed in this study. The evaluation results guide the separation and compensation of coupling aberrations in measurement. It is verified that the accuracy of a stitching CGH is considerably improved from 0.156λ to 0.017λ in terms of RMS after compensation. The findings obtained in this study during the development of stitching method and error evaluation are expected to promote the technology development and improvement of testing accuracy in stitching CGHs.

1. Introduction

Astronomical telescopes can expand human eyes and have become indispensable instruments in space exploration, earth imaging, and many other fields. With the increasing demands of high resolution and large field of view (FOV), modern telescopes are being developed for large-aperture primary mirrors. For example, the Large Synoptic Survey Telescope (LSST) is a large FOV survey telescope system with an 8.4 m primary mirror [1]. With an equivalent aperture of 24.5 m, the primary mirror of the Giant Magellan Telescope (GMT) consists of seven 8.4 m segmented mirrors [2].

Interferometric testing, a high-precision measurement technology, combined with computer-generated holograms (CGHs) has become the most efficient and widely used method for optical testing [3–8] and assisted alignment [9,10]. For optical testing and assisted alignment of extremely large aperture telescopes, it is vital to develop large-sized CGHs over 12 inches. However, these large-sized CGHs pose challenges on pattern accuracy and lithography equipment.

Generally, electron beam lithography [11] or laser direct writing [12] are used for CGH fabrication, yet it is difficult for electron beam lithography to achieve large-sized pattern plotting. Owing to the advantages of high scanning speed and exposure efficiency, laser direct writing lithography has been widely used in CGH fabrication. However, the capability of CGH fabrication commonly limits the maximum size of CGHs in the range of 6 to 9 inches, which obviously cannot satisfy the demand of large size.

In order to fabricate larger-sized CGHs, stitching becomes a feasible and necessary approach. To date, there has been few report on the use of stitching techniques for manufacturing larger-sized compensator CGHs. However, the stitching techniques have advanced considerably in the field of large-sized gratings. For example, scanning beam interference lithography is a widely used and mature technique that enables the large size of gratings by using scan-stitching techniques [13]. Massachusetts Institute of Technology has used this method to fabricate a meter-sized grating [14–15]. Inspiring from scan-stitching techniques, a multistep lithography method based on laser direct writing is proposed and implemented in this study to fabricate stitching CGHs.

As a wavefront compensator, it is vital for CGH to analyze the error sources and evaluate the testing accuracy. Some studies have been conducted on error analysis including fabrication [16–18], pattern dis-

* Corresponding authors.
E-mail addresses: zhangzhiyu@ciomp.ac.cn (Z. Zhang), zxj@ciomp.ac.cn (X. Zhang).

https://doi.org/10.1016/j.optlaseng.2021.106944
Received 2 September 2021; Received in revised form 18 November 2021; Accepted 29 December 2021
Available online 8 January 2022
0143-8166/© 2022 Elsevier Ltd. All rights reserved.

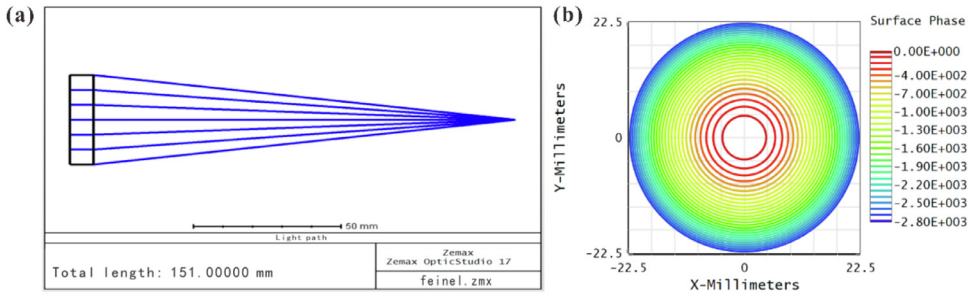

Fig. 1. Light path and surface pattern of the designed CGH.

tortion [19], encoding [20–22], and so on [23,24]. To measure the variations in duty cycle and etching depth of CGH, Cai et al. [25] developed a reconstruction device for a diffractive optics calibrator (DOC), while V.P. Korolkov from the Novosibirsk State University developed a novel spectrophotometric method to evaluate the uniformity of etching depth [26]. Murphy et al. proposed an interferometric method for measuring CGH imaging distortion [27]. Peterhänsel et al. discussed the limitations of applying scalar diffraction theory in CGH with sub-micron period and analyzed the sensitivity of the wavefront phase using the rigorous coupled wave theory [28]. However, few study has been published on the overlay errors of stitching.

For stitching CGHs, the primary errors are overlay errors introduced by stitching, which are bound to affect the testing accuracy. This evaluation work about the effects of overlay errors on wavefront has great significance for stitching CGHs. In this study, an evaluation method is established to analyze the wavefront aberrations introduced by stitching and the evaluation results are used for error compensation to improve the testing accuracy of stitching CGHs.

As a proof of concept, a stitching CGH with an aperture of 80 mm is designed and fabricated using multistep lithography to investigate the overlay errors. The pattern design, stitching method, and experimental flow are described in Section 2. Three kinds of overlay errors in stitching are analyzed and discussed in Section 3, and the theoretical derivation of evaluation model is provided in the supplemental document. In Section 4, the wavefront of an experimental stitching CGH is measured, and the measurement results are evaluated and compensated with respect to the overlay errors. The main conclusions are summarized in Section 5.

2. Experiment

2.1. Design of a stitching CGH

For experimental verification, a stitching CGH with three functional regions is designed on a substrate with diameter $D = 80$ mm and thickness $d = 8$ mm. The main region with a diameter of 45 mm represents the master hologram for testing a calibration ball. The focal length of the first diffraction order is $f_{cgh} = 143$ mm at wavelength $\lambda = 632.8$ nm. The light path and surface pattern designed by Zemax are shown in Fig. 1, and the period of fringe at the edge is about 240 lp/mm. The alignment region is used to align the CGH with the interferometer at the third reflection order. The alignment region ranges between diameters of 50 mm and 65 mm. Moreover, three circular holes are asymmetrically arranged in the main region for data processing and defocus adjustment.

A special positioning region is designed to assist the stitching process in secondary lithography, which is composed of cross marks and caliper rulers as shown in Fig. 2. The positioning region in stitching CGHs has two main functions. On the one hand, the calibration and determination of the center position between the multistep lithography processes are performed for stitching with the aid of the cross marks at the top and bottom of the same axis. On the other hand, the caliper rulers with different precisions (4 μm and 200 nm) are used to determine the overlay errors. The gray and blue patterns are drawn respectively by two-step lithography, and the final stitching caliper rulers are observed using a confocal microscope to measure the overlay errors.

Table 1
Fabrication parameters for the stitching CGH.

Items	Parameters
Laser energy/mW	105
Laser focus/mm	−40
CD bias/nm	−100
Photoresist thickness/nm	500
Chromium film thickness/nm	100
Processing stripe width/μm	80

2.2. Stitching procedure

Two-step lithography based on laser direct writing is developed to fabricate the stitching CGH, and its procedure is depicted in Fig. 3. The entire pattern is divided into two parts (pattern 01 and pattern 02) for stitching, and the diffraction microstructures of these patterns are fabricated on the same substrate.

First, a photoresist layer with a thickness of 500 nm is spin-coated onto the chrome-on-glass substrate. The initial half part (pattern 01) is completed after the first exposure, development, etching, and resist removal. The other half (pattern 02) is fabricated using the same process after recoating the photoresist and stitching. A laser scanning lithography system DWL4000 (Heidelberg Instruments Mikrotechnik GmbH, Germany) is used to write the patterns [29], and the fabrication parameters of setup are listed in Table 1.

In the above procedure, stitching needs to be performed between the first- and second- step lithography. A high-magnification microscope and the high-precision two-axis stage of DWL4000 are employed to perform stitching of patterns with the aid of cross marks shown in Fig. 2, and the stitching principle is shown in Fig. 4. After the first-step lithography, the CGH with pattern 01 is re-placed on the two-axis stage, and θ is the angle deviation between the coordinate *x'oy'* of the CGH and the coordinate *xoy* of the stage. A pair of cross marks on the *x'* or *y'* axis are searched in pattern 01 by using the microscope, and their center coordinates (x_1, y_1) and (x_2, y_2) are determined in the *xoy*-plane. The angle deviation θ is equal to $\arctan((x_1 - x_2)/(y_1 - y_2))$, which is corrected in the second-step lithography through the rotation of pattern 02. The center of the CGH pattern is setup at $(\frac{x_1+x_2}{2}, \frac{y_1+y_2}{2})$ for the second-step lithography.

2.3. Error evaluation

CGH plays a primary role in determining the accuracy of optical testing; therefore, error evaluation of the stitching CGH is necessary. The error evaluation includes the measurement of overlay errors resulting from the stitching procedure and the wavefront accuracy of the stitching CGH.

First, a confocal microscope (Olympus, OLS 4100) is used to observe the caliper rulers under a 50 × magnification objective lens, as shown in

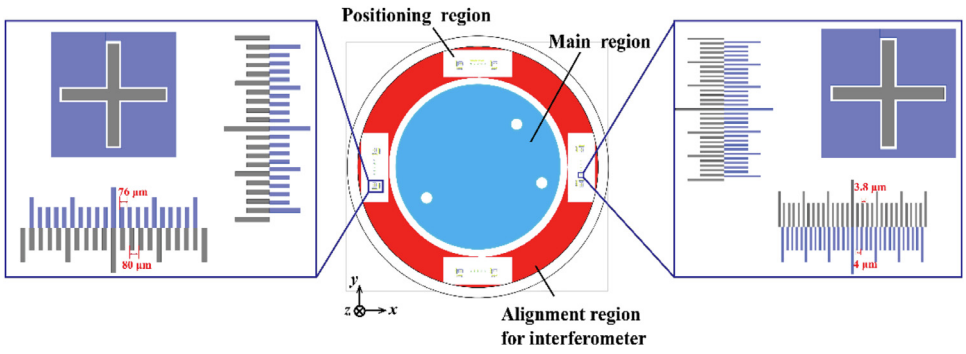

Fig. 2. Distribution of functional regions and pattern design of positioning region.

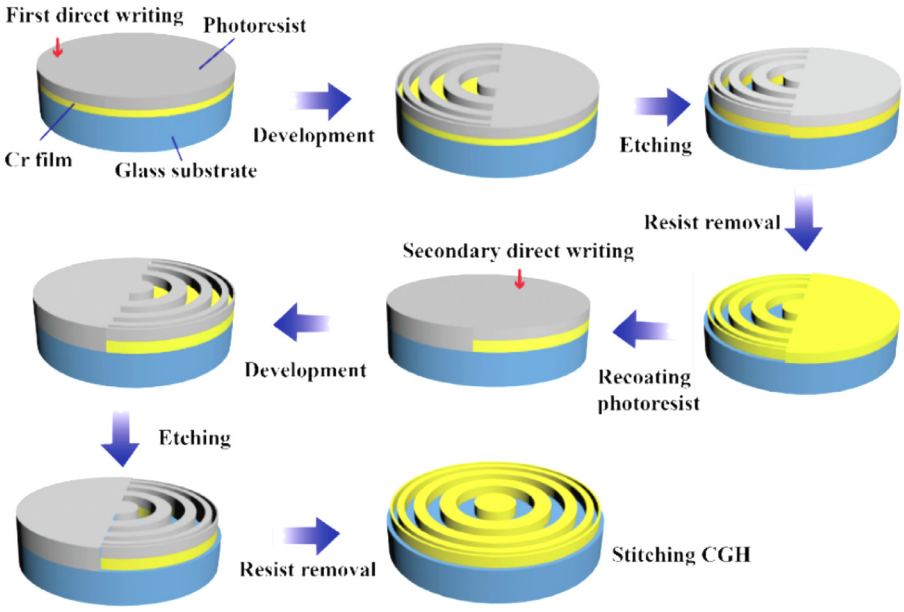

Fig. 3. Fabrication procedure of two-step lithography for a stitching CGH.

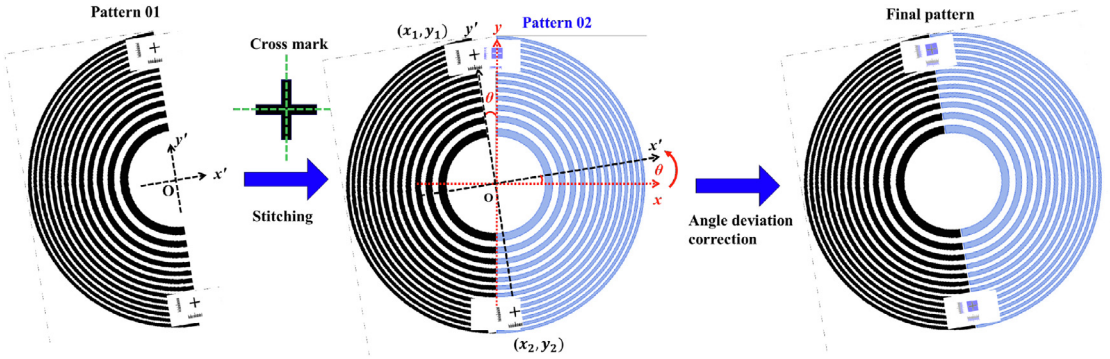

Fig. 4. Principle of pattern stitching and calibration process.

Fig. 5. The gray and blue patterns of the caliper rulers are plotted based on the above two-step lithography. The transverse and longitudinal deviations can be determined from the alignment of the comb-teeth of the rulers, and the measurement accuracy is 200 nm.

Second, a schematic of the optical path for evaluating the wavefront aberrations of the stitching CGH is illustrated in Fig. 6, and the experimental setup is depicted in Fig. 7. In this setup, a calibration ball with extremely high precision (0.6 nm RMS), which is considerably higher than the accuracy of CGH, is used as the test surface. Thus, the test results can directly represent the wavefront accuracy of the CGH. The design parameters of the light path are listed in Table 2.

3. Analysis of overlay errors in stitching

In this section, the wavefront aberrations induced by the overlay errors in stitching CGHs are discussed and simulated. In Fig. 8(a), pattern 01 is completed by first-step lithography, and its coordinate system $x_R o_R y_R$ is taken as a reference. Stitching pattern 02 with errors determines the actual coordinate system $x_E o_E y_E$. A schematic diagram of the coordinate transformation of the stitching pattern between the actual and ideal is shown in Fig. 8(b).

In the stitching process, because the two parts of the holographic patterns are drawn on the same substrate, there is no translation error along the z-axis. Overlay errors of stitching can be described by the

Table 2
Parameters of experimental light path.

Items	Parameters
Wavelength λ	632.8 nm
Reference sphere $F\#$	3.3
Focal length of reference sphere f_0	330 mm
Focal length of CGH f_{cgh}	143 mm
Distance from focal plane to CGH u	500 mm
Distance from CGH to calibration ball v	200 mm

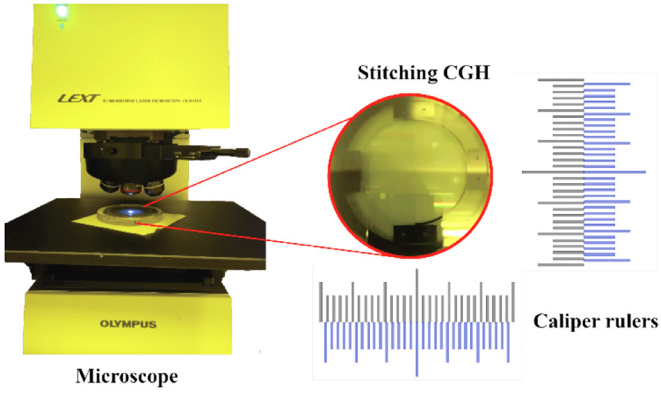

Fig. 5. Measurement method of overlay errors in stitching CGHs.

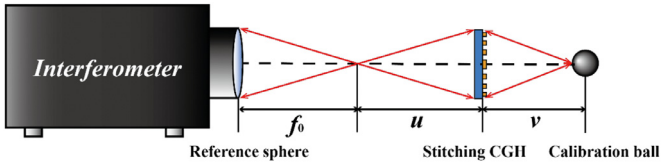

Fig. 6. Optical path for wavefront measurement of the stitching CGH.

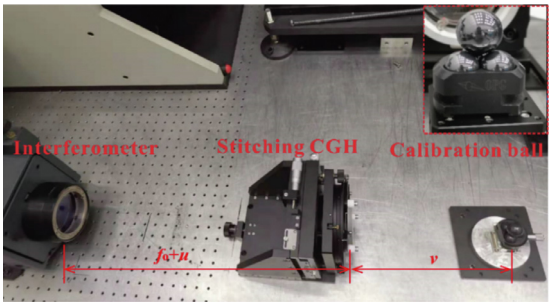

Fig. 7. Experimental setups for wavefront measurement of the stitching CGH.

transverse deviation a (Fig. 9(a)), longitudinal deviation b (Fig. 9(b)), and rotation angle deviation γ ((Fig. 9(c)).

For a stitching CGH with these overlay errors, the relationship between (x_E, y_E) and (x_R, y_R) can be expressed as follows:

$$\begin{pmatrix} x_E \\ y_E \end{pmatrix} = \begin{pmatrix} \cos\gamma & -\sin\gamma \\ \sin\gamma & \cos\gamma \end{pmatrix} \begin{pmatrix} x_R \\ y_R \end{pmatrix} + \begin{pmatrix} a \\ b \end{pmatrix} \tag{1}$$

The transmittance function of the designed CGH can be expressed as

$$t(x_R, y_R) = \exp\left[-\frac{ik}{2f_{cgh}}({x_R}^2 + {y_R}^2)\right] \tag{2}$$

The transmittance function of a stitching CGH with overlay errors is modified as

$$\begin{aligned} t(x_E, y_E) &= \exp\left\{-\frac{ik}{2f_{cgh}}\left\{\left[(x_E - a)\cos\gamma + (y_E - b)\sin\gamma\right]^2\right.\right. \\ &\quad \left.\left. + \left[(y_E - b)\cos\gamma - (x_E - a)\sin\gamma\right]^2\right\}\right\} \\ &= \exp\left\{-\frac{ik}{2f_{cgh}}\left[(x_E - a)^2 + (y_E - b)^2\right]\right\} \end{aligned} \tag{3}$$

There is no parameter γ (rotation angle deviation) in the above equation. It means that the transmittance function of a stitching CGH is independent of γ, and therefore the rotation error has no effect on the wavefront. In addition, the rotation error originates mainly from the orthogonality error between the guide rails of the lithography equipment, which has been calibrated to less than 0.2 μrad. Thus, the rotation angle deviation of a stitching CGH can be ignored, and the following discussion will focus on the overlay errors of transverse and longitudinal deviations.

Next, a parameter model is established to evaluate the effects of overlay errors on wavefront according to the designed light path, as shown in Fig. 10. It is known that the wavefront returning to interferometer through a perfect CGH must be an ideal plane wave without phase errors [30], and the derivation is described in Part A of the supplementary document.

In Fig. 11, an overlay error in the transverse deviation a is introduced into the evaluation model. The propagation of the reflected light from the calibration ball through the initial half (pattern 01) as reference is indicated by a green line, and that through the other half with transverse deviation a is indicated by a red line. For a stitching CGH, the initial half, which is taken as reference, is regarded as part of a perfect CGH, so the wavefront aberrations caused by the overlay errors will exist in the stitching half part.

According to Eq. (3), the transmittance function of a stitching CGH with transverse deviation a can be modified as

$$t(x_E, y_E) = \exp\left\{-\frac{ik}{2f_{cgh}}\left[(x_E - a)^2 + {y_E}^2\right]\right\} \tag{4}$$

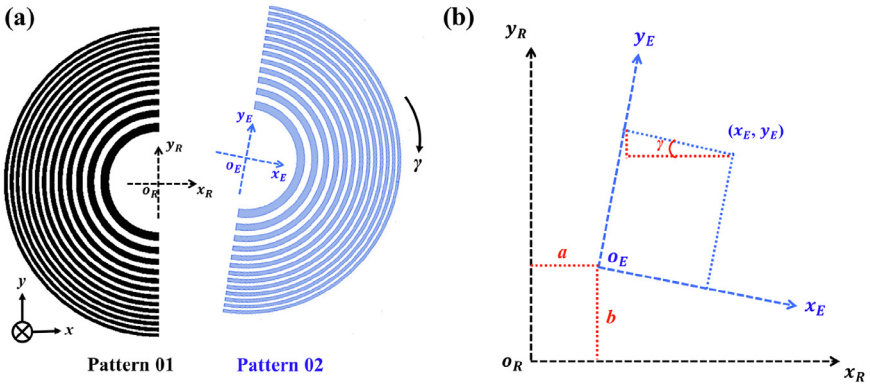

Fig. 8. (a) The mismatch problem of a stitching CGH with overlay errors. (b) Schematic diagram of coordinate transformation of stitching patterns.

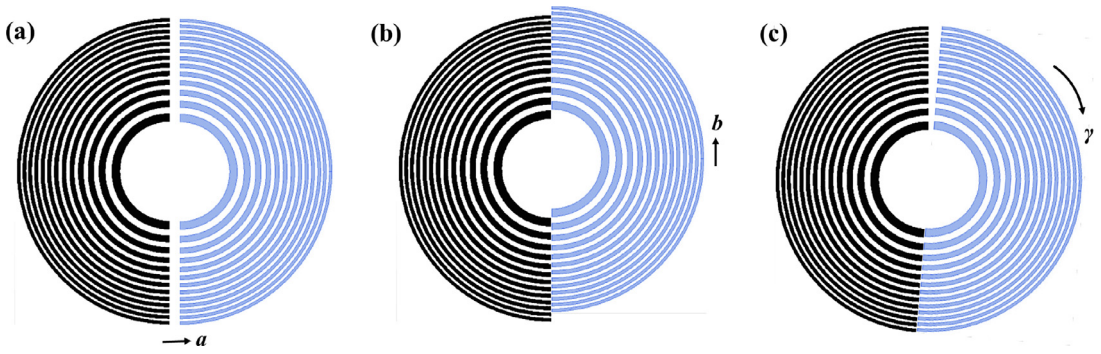

Fig. 9. Overlay errors of (a) transverse deviation a, (b) longitudinal deviation b and (c) rotation angle deviation γ.

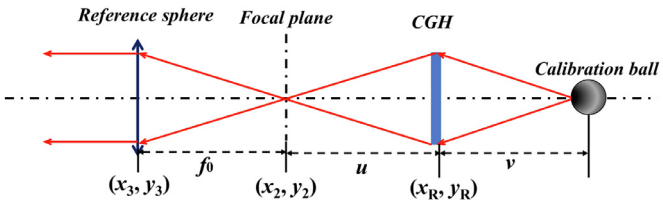

Fig. 10. Layout of parameter model for wavefront evaluation.

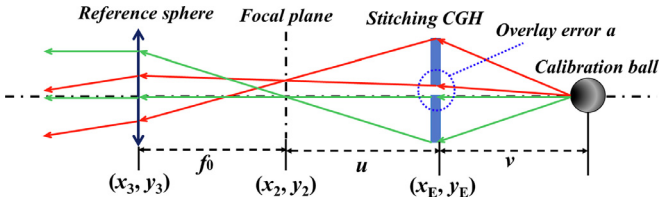

Fig. 11. Layout of the evaluation model for a stitching CGH with transverse deviation a.

The final wavefront through a stitching CGH with transverse deviation a is described as

$$U_4'(x_3, y_3) = A_0 \exp\left\{-\frac{ik}{f_0}\left[\frac{au}{f_{cgh}}x_3 - \left(\frac{au}{f_{cgh}}\right)^2\right]\right\} \tag{5}$$

Eq. (5) indicates that transverse deviation a causes tip aberration in the wavefront of the stitching part, and the phase error $\phi_t(x_3, y_3)$ can be expressed as

$$\phi_t(x_3, y_3) = -\frac{2\pi}{\lambda}\left(\frac{au}{f_0 f_{cgh}}x_3\right) \tag{6}$$

As for longitudinal deviation b introduced into the stitching part, the conclusion is similar to that of transverse deviation based on above evaluation model. The transmittance function can be expressed as

$$t(x_E, y_E) = \exp\left\{-\frac{ik}{2f_{cgh}}\left[{x_E}^2 + (y_E - b)^2\right]\right\} \tag{7}$$

The obtained final wavefront with tilt aberration can be written as

$$U_4'(x_3, y_3) = A_0 \exp\left\{-\frac{ik}{f_0}\left[\frac{bu}{f_{cgh}}y_3 - \left(\frac{bu}{f_{cgh}}\right)^2\right]\right\} \tag{8}$$

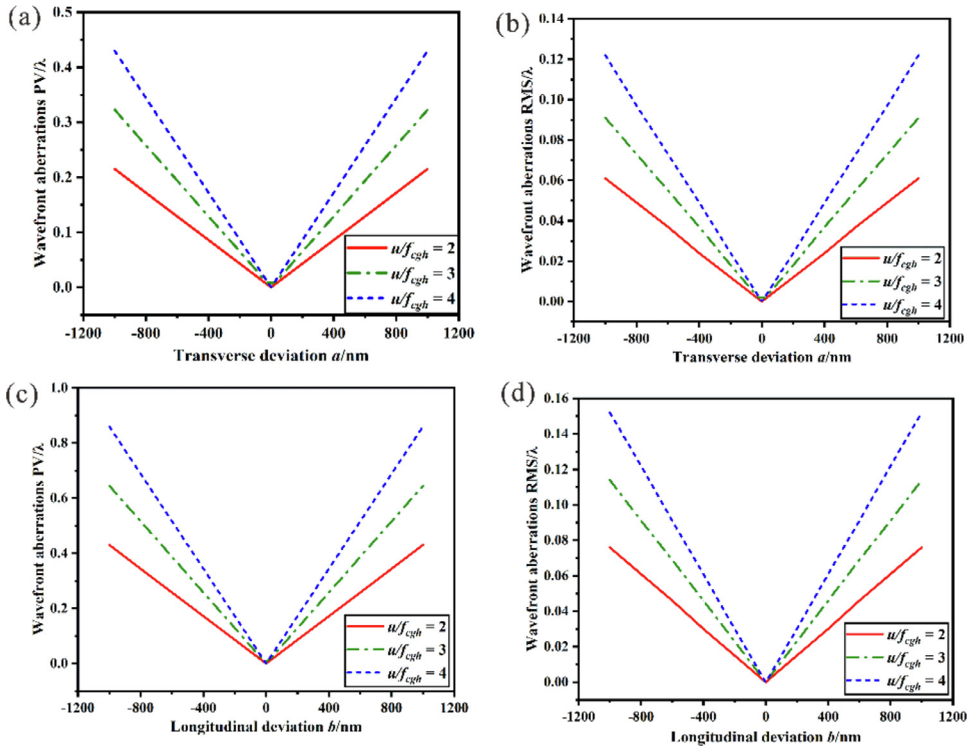

Fig. 12. Wavefront aberrations induced by various transverse and longitudinal deviations.

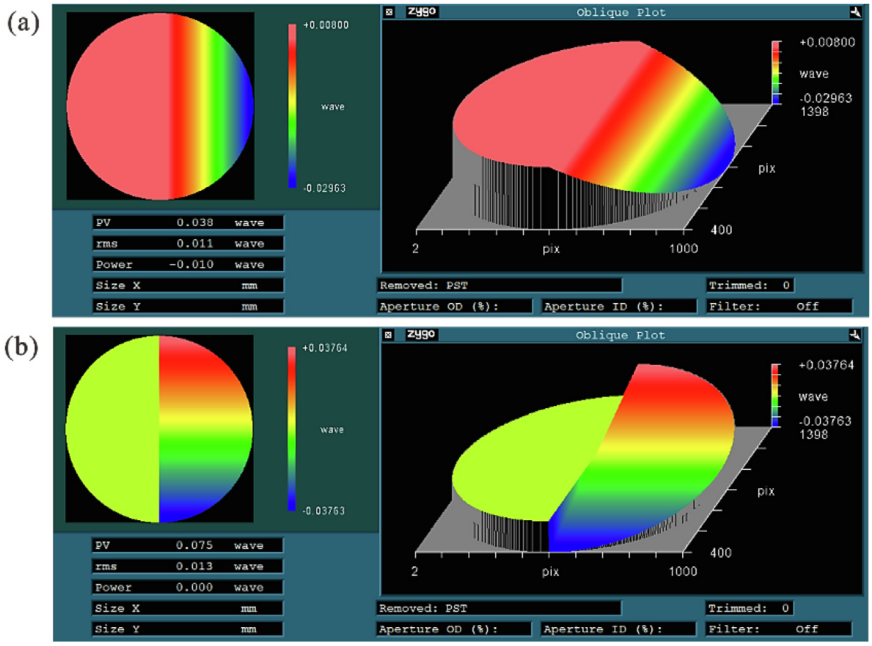

Fig. 13. Wavefront aberration caused by 100 nm deviation in (a) transverse direction or (b) longitudinal direction.

The phase error caused by longitudinal deviation b in a stitching CGH is

$$\phi_l(x_3, y_3) = -\frac{2\pi}{\lambda}\left(\frac{bu}{f_0 f_{cgh}} y_3\right) \tag{9}$$

The theoretical derivation of the above conclusions about overlay errors has been provided in the supplemental document. In Eq. (6) and Eq. (9), the coefficient of the phase error is determined by the design parameters of CGH (u, f_{cgh}) and overlay errors (transverse or longitudinal deviation). The wavefront aberrations induced by various overlay errors for several different CGH designed parameters u/f_{cgh} are calculated, and the results are plotted in Fig. 12.

These results reveal a linear relationship between the PV or RMS values of the wavefront aberrations and overlay errors. Compared with the results of transverse and longitudinal deviations, the PV value of the aberrations with the same amount of deviation in the longitudinal direction is approximately twice that in the transverse direction. This is because the PV value of the tip/tilt aberration is determined by the effective aperture, and the effective aperture of the stitching part in the longitudinal direction of the tilt is a full-aperture, whereas that in the transverse direction of the tip is a half-aperture for a stitching CGH.

In addition, the aberration caused by overlay errors appears more sensitive with the increase in the ratio of design parameters u and f_{cgh}. The impact of overlay errors on the wavefront depends on the design parameters of stitching CGHs; therefore, they need to be analyzed and evaluated according to specific design parameters.

According to Section 2, the design parameters of the stitching CGH are u = 500 mm, f_0=330 mm, f_{cgh}=143 mm, aperture D = 45 mm and λ=632.8 nm. The wavefront aberrations caused by the transverse and longitudinal deviations of 100 nm are simulated, and the evaluation results are shown in Fig. 13. The tip aberration (Fig. 13(a)) with 0.038λ PV and 0.011λ RMS results from the transverse deviation in the stitching CGH, and the tilt aberration (Fig. 13(b)) with 0.075λ PV and 0.013λ RMS results from the longitudinal deviation. Thus, when the required wavefront accuracy is less than 0.01λ in terms of RMS for the stitching CGH, the overlay errors in the transverse or longitudinal direction must not exceed 100 nm. However, the impact of overlay errors cannot be ignored due to the limitation of stitching accuracy; hence, it is necessary to evaluate and calculate them for error compensation.

As expected, these two forms of overlay errors introduce a tip/tilt aberration in the wavefront. However, it is known that tip/tilt aberrations are often caused by adjustment errors during measurement of the CGH and test surface [31]. The aberrations induced by overlay errors and adjustment errors may be coupled, which makes it hard to directly measure the effect of overlay errors. Hence, there is great significance in developing a method to evaluate overlay errors by simulation. The above evaluation method is established to budget the wavefront aberrations caused by overlay errors for a stitching CGH, and the flowchart is summarized in Fig. 14.

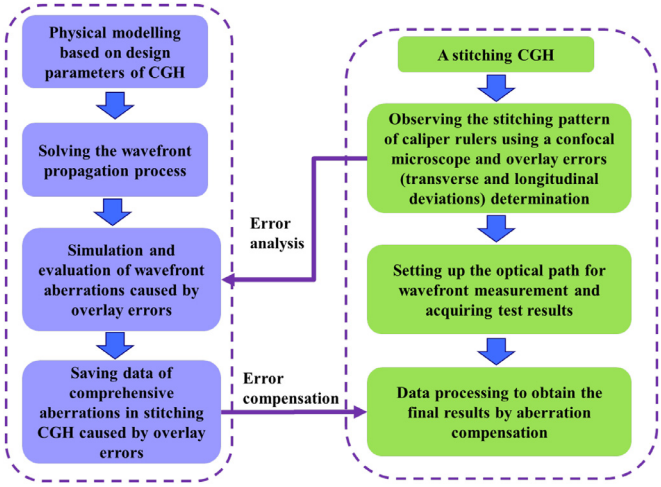

Fig. 14. The flow of evaluation method for overlay errors in stitching CGHs.

First, a physical model is established based on the design parameters to evaluate the effects on the wavefront for a stitching CGH with overlay errors. Next, the quantitative relationships between aberrations and overlay errors are obtained by deriving the propagation process of the wavefront. The overlay errors including transverse deviation and longitudinal deviation of stitching fringes are measured through observing caliper rulers with a microscope. Finally, the wavefront aberrations caused by these overlay errors are simulated and budgeted based on the evaluation model, and they are compensated and corrected in the measurement results to improve the testing accuracy.

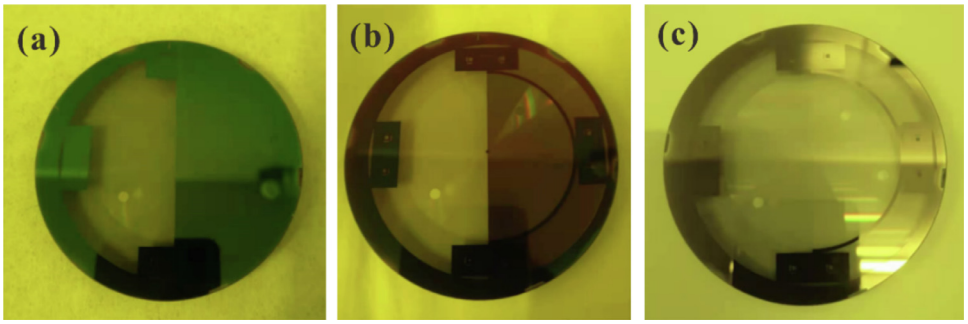

Fig. 15. (a) Initial half pattern of the stitching CGH. (b) Stitching CGH after secondary exposure and development. (c) Final stitching CGH.

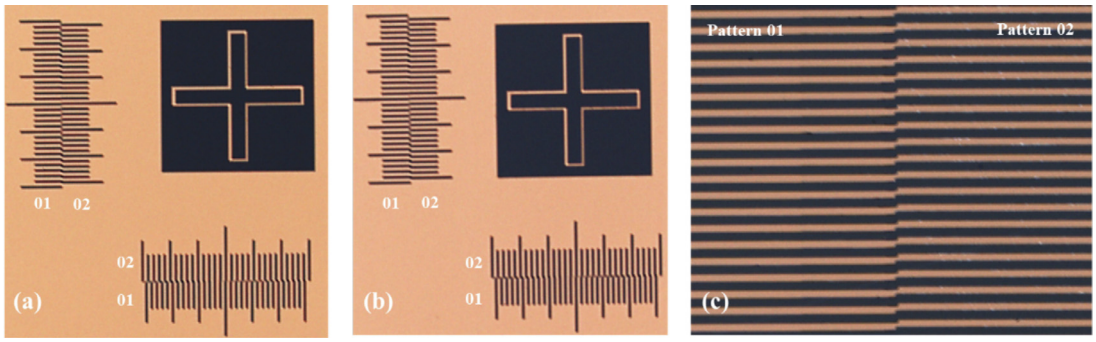

Fig. 16. Overlay error measurement. Top (a) and bottom (b) stitching patterns (caliper rulers). (c) Local fringe pattern at CGH suture.

4. Results

4.1. Fabrication of a stitching CGH

The following images depict the several steps of the fabrication of our experimental CGH using the stitching method described in Section 2. Fig. 15(a) illustrates the product obtained after the first-step lithography, which has been then recoated with a photoresist layer. Fig. 15(b) depicts the stitching pattern after secondary exposure and development. Subsequently, the final etching and resist removal are performed to obtain a stitching CGH, as shown in Fig. 15(c).

4.2. Measurement of overlay errors

In this section, the overlay errors are measured, which are served for the evaluation and compensation of wavefront aberrations of the stitching CGH in Section 4.4. Fig. 16 depicts parts of the final patterns in this experimental stitching CGH. The black fringes represent the transmitted

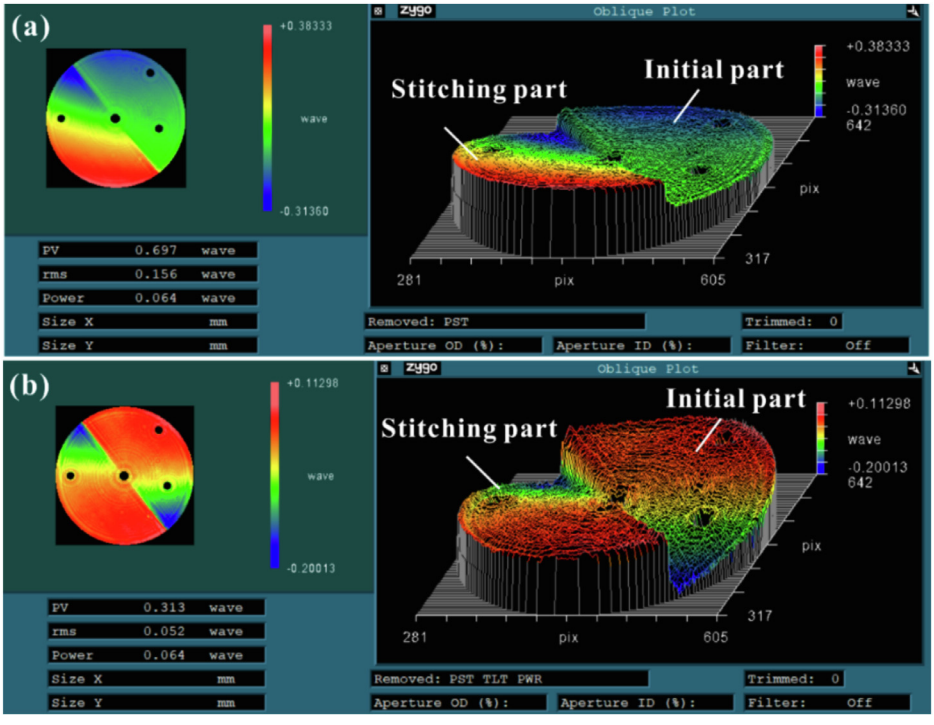

Fig. 17. Wavefront aberrations of stitching CGH: (a) subtracting piston, and (b) subtracting piston and tilt.

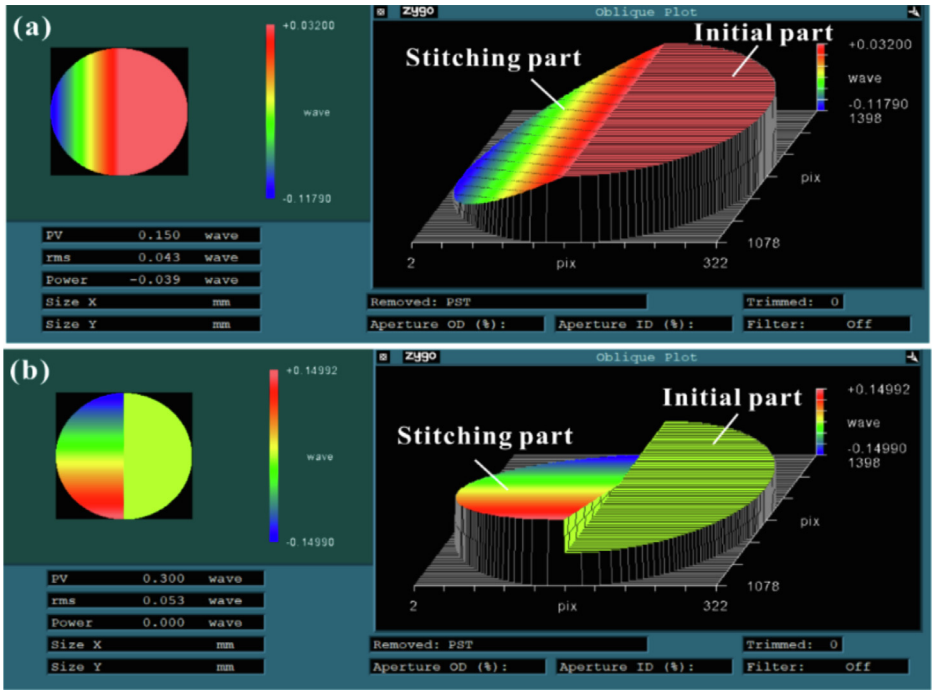

Fig. 18. Wavefront aberration evaluation. (a) 400 nm transverse deviation. (b) 400 nm longitudinal deviation.

region through exposure and etching, and the gold fringes represent the remaining chromium microstructure. In the positioning region, a pair of cross marks and caliper rulers were observed using a microscope in the longitudinal direction, and the top and bottom patterns are depicted in (a) and (b), respectively. According to the dislocation of the comb-teeth of the rulers, there are approximately 400 nm deviations in both the transverse and longitudinal directions, which cause the dislocation of the stitching pattern, as depicted in Fig. 16(c). The comparison of the top and bottom measurement results reveals that the errors are almost the same, indicating that the deviation of the rotation angle is negligible and can thus be ignored.

4.3. Wavefront measurement

Based on interferometric testing, the measurement result of the stitching CGH shown in Fig. 17 was obtained. The stitching half exhibited a significant tilt aberration in the wavefront depicted in Fig. 17(a). Because tip/tilt and defocus aberrations are often caused by adjustment

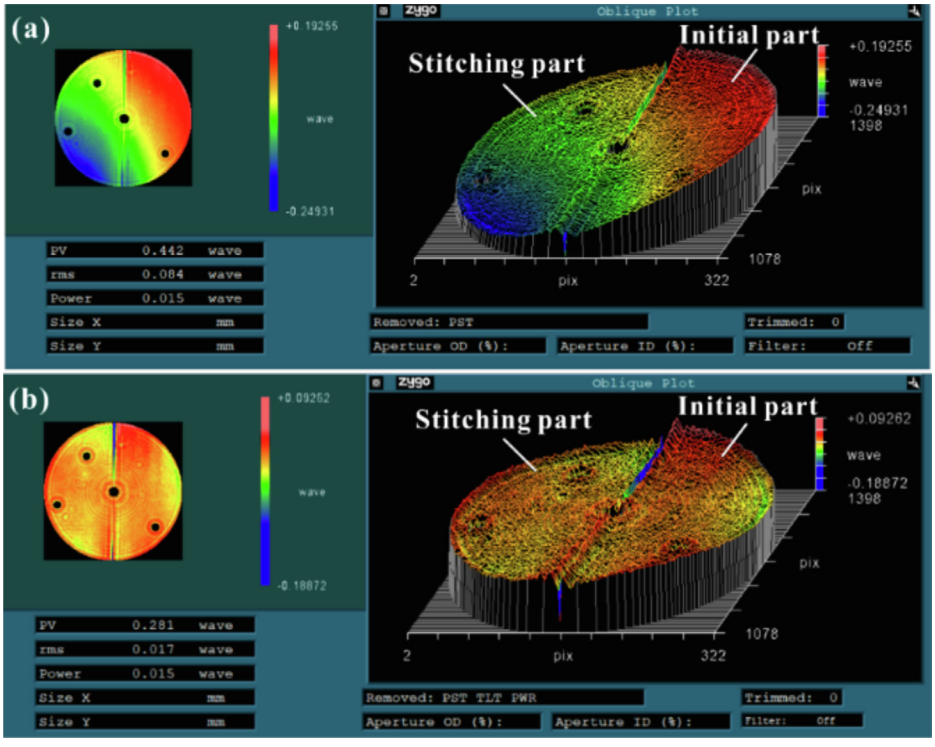

Fig. 19. (a) Residual wavefront aberrations after the compensation of aberrations induced by the overlay errors. (b) Final result after subtracting tilt and defocus induced by the adjustment errors.

errors, they are typically supposed to be directly subtracted. The wavefront obtained after subtracting the tip/tilt and defocus aberrations is illustrated in Fig. 17(b), which shows that the wavefront of the entire aperture is severely distorted. This phenomenon is attributed to the coupling of the tip/tilt aberrations induced by the overlay errors and adjustment errors. Thus, it is necessary to separate the coupling aberrations through error evaluation rather than subtraction, as mentioned above. The experimental results reveal that it is unreasonable to directly subtract the tip/tilt aberrations in the interferometric optical testing based on stitching CGHs.

4.4. Evaluation and compensation of overlay errors

In Sections 4.2 and 4.3, it is known that the measurement result of the stitching CGH depicted in Fig. 17(a) includes the aberrations induced by the 400 nm transverse deviation, 400 nm longitudinal deviation, and adjustment errors. By using the evaluation method established in Section 3, the aberrations induced by overlay errors are simulated and calculated as shown in Figs. 18(a) and (b). The simulation is based on the following parameters of the stitching CGH: u = 500 mm, f_0 = 330 mm, f_{cgh} = 143 mm, aperture D = 45 mm and λ = 632.8 nm.

Based on the evaluation results, the aberration compensation is conducted as follows. The tip-tilt aberrations caused by the overlay errors are compensated into the measurement result, and Fig. 19(a) depicts the result of subtracting the evaluation results in Figs. 18(a) and (b) from the measurement result in Fig. 17(a).

The wavefront after compensation exhibits a global residual tilt aberration, as illustrated in Fig. 19(a), which is caused by the adjustment errors that can be directly subtracted. After subtracting the residual tilt and defocus aberrations, the wavefront of the stitching CGH obtained is shown in Fig. 19(b). The result obtained after overlay error compensation can reach 0.017λ in terms of RMS, which represents a significant improvement compared with the initial wavefront. The stitching trace can still be observed in the final result, because these overlay errors cause a gap at the suture, and the interferometer has limitations in the testing of the wavefront with step characteristics. Thus, the trace cannot be completely eliminated by the wavefront aberration compensation. The residual wavefront aberrations in Fig. 19(b) after compensation can be attributed to comprehensive errors, including the fabrication, substrate, and measurement errors.

Through the above evaluation and compensation of overlay errors, it is verified that the accuracy of the stitching CGHs can be better than 1/50λ. This accuracy of the stitching CGH can meet the requirement of the optical systems. If the stitching accuracy of the equipment and measurement accuracy of the overlay errors are further improved, stitching CGHs can reach higher accuracy.

Moreover, the evaluation of the wavefront aberrations induced by the overlay errors has great significance in the development of the stitching technology and accuracy improvement of the stitching CGHs. These evaluation results serve as compensation references to guide the subsequent aberration correction; in contrast, it is difficult for a stitching CGH without error compensation to meet the high accuracy requirements. In this study, the stitching technology and error evaluation method are developed and practiced through experiments, verifying the feasibility of large-sized stitching CGHs.

5. Conclusion

In this study, a novel multistep lithography method was developed to achieve large-sized stitching CGHs, and an experimental CGH was fabricated for errors investigation. Experimental results show that stitching process introduces overlay errors into patterns, which cause the additional tip/tilt aberrations into the wavefront. However, the aberrations from overlay errors are coupled with that from adjustment errors in measurement, which directly affects the testing accuracy of stitching CGHs. To separate and compensate the coupling aberrations, an evaluation method is proposed and implemented in experimental results, and the accuracy of the stitching CGH has considerably improved from 0.156λ to 0.017λ in terms of RMS. The accuracy of stitching CGHs can well satisfy the requirements of optical systems. With the development of lithography techniques, the stitching accuracy are expected to be further improved. Large-sized stitching CGHs with high accuracy would be realized based on the development multistep lithography and compensation methods, which has great significance in the testing of large-scale optical systems and the development of extremely large telescopes. In our future work, we intend to fabricate a high-precision stitching CGH with a large aperture of 600 mm using this method (Eqs. 1, 2, 4, 7, 8).

Fundings

This work was supported by the National Natural Science Foundation of China (51775531, 11803037). This work was partially supported by the Advanced Science Key Research Project of the Chinese Academy of Science (QYZDJ-SSW-JSC038) and Key Foreign Cooperation Projects of International Cooperation Bureau, Chinese Academy of Science (181722KYSB20180015).

Declaration of Competing Interest

The authors declare no conflicts of interest.

Supplementary materials

Supplementary material associated with this article can be found, in the online version, at doi:10.1016/j.optlaseng.2021.106944.

References

[1] Araujo-Hauck C, Sebag J, Liang M, Neill D, Muller G, Thomas SJ, Vucina T, Gressler WJ. LSST mirror system status: from design to fabrication and integration. Ground-Based & Airborne Telescopes Vi. Ground-Based and Airborne Telescopes 2016. doi:10.1117/12.2232923.
[2] Zhou P, Martin HM, Zhao C, Burge JH. Mapping distortion correction for GMT interferometric test. Optical Fabrication & Testing 2012. doi:10.1364/OFT.2012.OW3D.2.
[3] Burge JH, Zhao C, Dubin M. Measurement of aspheric mirror segments using Fizeau interferometry with CGH correction. Proc SPIE Int Soc Opt Eng 2015:7739. doi:10.1117/12.857816.
[4] Li S, Zhang J, Liu W, Guo Z, Li H, Yang Z, et al. Measurement investigation of an off-axis aspheric surface via a hybrid compensation method. Appl Opt 2018;57(28):8220–7. doi:10.1364/AO.57.008220.
[5] Masaru K, Kurita M. Interferometric testing for off-axis aspherical mirrors with computer-generated holograms. Appl Opt 2012;51(19):4291–7. doi:10.1364/AO.51.004291.
[6] Yang HS, Song JB, Lee IW, Lee YW. Testing of steep convex aspheric surface with a hartmann sensor by using a CGH. Opt Exp 2006;14(8):3247. doi:10.1364/OE.14.003247.
[7] Ji B, Yan H, Shi Q, Wen S. Comparison of aspherical wave-front measurement by null compensator and computer-generated holograms. Conference on Optics Ultra Precision Manufacturing and Testing; 2020. doi:101117/122580418.
[8] Peng J, Chen Z, Zhang X, Fu T, Ren J. Optimal design of tilt carrier frequency computer-generated holograms to measure aspherics. Appl Opt 2015;54(24):7433–41. doi:10.1364/AO.54.007433.
[9] Zhang X, Hu H, Xue D, Li M. Testing and alignment of freeform-based multi-mirror telescopes. SPIE Opt Eng Appl Int Soc Opt Photon 2015. doi:10.1117/12.2189967.
[10] Song H, Hao X, Huang J, Jiang W. Detection technology for co-phasing segmented primary mirrors based on broadband interferometric system. Qiangjiguang Yu Lizishu High Power Laser Part. Beams 2008;20(1):41–4.
[11] Arnold SM. Electron beam fabrication of computer-generated holograms. Opt Eng 1985;24(5):803–7. doi:10.1117/12.7973578.
[12] Miao J, Ding X, Zhou S, Gui C. Fabrication of dynamic holograms on polymer surface by direct laser writing for high-security anti-counterfeit applications. IEEE Access 2019;PP(99):1 1. doi:10.1109/ACCESS.2019.2944838.
[13] Ma D, Zhao Y, Zeng L. Achieving unlimited recording length in interference lithography via broad-beam scanning exposure with self-referencing alignment. Sci Rep 2017;7(1):926. doi:10.1038/s41598-017-01099-3.
[14] Chen CG, Konkola PT, Heilmann RK, Joo C, Schattenburg ML, "Nanometer-accurate grating fabrication with scanning beam interference lithography," Proc. SPIE 4936, 126–134 (2002). doi:10.1117/12.469431.
[15] Zhao Y. [Doctoral dissertation]. Massachusetts Institute of Technology; 2008.

[16] Gan Z, Peng X, Chen S, Guan C, Hu H, Li X, et al. Fringe discretization and manufacturing analysis of a computer-generated hologram in a null test of the freeform surface. Appl Opt 2018;57(34):9913–21. doi:10.1364/AO.57.009913.
[17] Chang Y, Zhou P, Burge JH. Analysis of phase sensitivity for binary computer-generated holograms. Appl Opt 2006;45(18):4223–34. doi:10.1364/AO.45.004223.
[18] Lin H, Chen S, Shuai X. Characterization of the contribution of CGH fabrication error to measurement uncertainty in null test. AOPC 2017: Optoelectronics and Micro/Nano-Optics 2021.
[19] Gan Z, Peng X, Chen S, Guan C. Evaluation of wavefront errors introduced by pattern distortion of computer-generated holograms. Opt Int J Light Electron Opt 2019;185:699–706. doi:10.1016/j.ijleo.2019.04.007.
[20] Zhao C, Burge JH. Generalization of the Coddington equations to include hybrid diffractive surfaces. Proc SPIE Int Soc Opt Eng 2010;7652. doi:10.1117/12.871853.
[21] Cai W, Zhou P, Zhao C, Burge JH. Analysis of wave-front errors introduced by encoding computer-generated holograms. Appl Opt 2013;52(34):8324–31. doi:10.1364/AO.52.008324.
[22] Xiao X, Yu Q, Zhu Z, Kai H, Chen G. Encoding method of cgh for highly accurate optical measurement based on non-maxima suppression. Chin Opt Lett 2017;15(011):41–5. doi:10.3788/COL201715.111201.
[23] Reichelt S, Pruss C, Tiziani HJ, Osten W. Specification and characterization of CGHs for interferometrical optical testing. Interferometry Xi: Applications, SPIE 2002;4778:206–17. doi:10.1117/12.473540.
[24] Stephan S. Error compensation in computer generated hologram-based form testing of aspheres. Appl Opt 2014;53(35):8249–55. doi:10.1364/AO.53.008249.
[25] Cai W, Zhou P, Zhao C, Burge JH. Diffractive optics calibrator: measurement of etching variations for binary computer-generated holograms. Appl Opt 2014;53(11):2477–86. doi:10.1364/ao.53.002477.
[26] Korolkov VP, Konchenko AS, Cherkashin VV. Etch depth mapping of phase binary computer-generated holograms by means of specular spectroscopic scatterometry. Opt Eng 2013;52(9):72. doi:10.1117/1.OE.52.9.091722.
[27] Murphy PE, Brown TG, Moore DT. Measurement and calibration of interferometric imaging aberrations. Appl Opt 2000;39(34):6421–9. doi:10.1364/AO.39.006421.
[28] Peterhänsel S, Pruss C, Osten W. Phase errors in high line density CGH used for aspheric testing: beyond scalar approximation. Opt Express 2013;21(10):11638–51. doi:10.1364/OE.21.011638.
[29] Guo C, Zhang Z, Xue D, Li L, Wang R, Zhou X, et al. High-performance etching of multilevel phase-type Fresnel zone plates with large apertures. Opt Commun 2018;407:227–33. doi:10.1016/j.optcom.2017.09.006.
[30] Goodman JW. Introduction to fourier optics. McGraw-Hill; 1968.
[31] He Y, Hou X, Qiang C, Fan W, Song W. Analysis of adjustment error in aspheric null testing with CGH. Optical Test. 8th International Symposium on Advanced Optical Manufacturing and Testing Technologies: Optical Test, Measurement Technology, and Equipment; 2016.